Application of the Unequal Distances of Closest Approach Theory to the Analysis of Double-Layer Effects on Zn(II) Reduction at a Mercury Electrode

G. López-Pérez, R. Andreu,* D. González-Arjona, M. Molero, and J. J. Calvente

Department of Physical Chemistry, University of Seville, Seville E-41012, Spain

Received: April 12, 2001; In Final Form: June 25, 2001

The orthogonal collocation technique has been applied to the development of a numerical solution of the unequal distances of closest approach (UDCA) theory for any number of electrolytes and planes of closest approach to the electrode surface. On the basis of theoretical analysis of the reaction coordinate of Zn^{2+} reduction by Schmickler et al. (*Chem. Phys.* **2000**, *252*, 349), a UDCA analysis of the Frumkin effect on the observed charge-transfer rate constants has been performed. The supporting electrolytes $LiClO_4$, $Mg(ClO_4)_2$, and $Al(ClO_4)_3$ were chosen to vary systematically the distance of closest approach of the electrolyte cation with respect to that of the electroactive species. UDCA distances of closest approach derived from electrocapillary data are shown to provide a reasonable account of the Frumkin effect. However, more consistent results are obtained when variations of the Zn^{2+} activity coefficient, computed from the MSA theory, are also considered.

Introduction

The reduction of Zn^{2+} at a mercury electrode is one of the most extensively studied reactions in electrochemistry, but some important aspects of its mechanism have remained controversial. Thus, whereas some authors have favored an ion-transfer approach to describe the amalgamation process,[1,2] an alternative mechanism including two consecutive electron-transfer steps appears to provide a more direct explanation of the charge-transfer rate constant dependence on electrode potential.[3−6] Some recent work of Schmickler et al.[7,8] supports the latter option from a theoretical point of view, at least when Zn^{2+} is being reduced from an aqueous solution, due essentially to the high energetic cost required for the full dehydration of Zn^{2+}. Their molecular dynamics simulations show that the minimum-energy reaction path involves the presence of a less hydrated Zn^{+} intermediate, whose distance of closest approach to the electrode is smaller than that of Zn^{2+}. The reaction mechanism can then be envisaged as a series of two one-electron-transfer steps, including partial dehydration and penetration of the reactants through the double layer, in qualitative agreement with the conclusions reached from a previous analysis of the charge-transfer rate constant variation with the water activity.[5] In light of the new theoretical evidence, our purpose in this work is to explore the influence of the double-layer structure on the rate of Zn^{2+} reduction, accounting for the local average potential values at the two planes where the electroactive species are expected to be located.

The catalytic influence of the interfacial structure on the rate of charge-transfer reactions is usually discussed in terms of the Frumkin effect.[9] Within the framework of the Gouy−Chapman−Stern electrostatic description of the double layer, the Frumkin effect accounts for changes of both the reactant concentration at the discharge plane and the effective driving potential, when the supporting electrolyte is varied. In an earlier analysis of the Zn^{2+} reduction in the presence of $NaClO_4$,[5] it was concluded that the usual hypothesis of the equal location of the planes of closest approach of all ions in solution leads to an overcorrection of the double-layer effect. In fact, more satisfactory results were obtained by assuming that the strongly solvated Zn^{2+} cation could not approach the electrode as close as the less solvated Na^{+} ion, so that the potential at the reaction plane was less negative than the potential at the outer Helmholtz plane of the electrolyte. The implications of this type of approach, in which the reactant adapts itself to a Gouy−Chapman potential profile set by the background electrolyte, have been reviewed by Fawcett.[10] However, a theoretical description of the double layer that recognizes separate distances of closest approach for each ion, and that treats on an equal footing the reactant and the electrolyte ions,[11] seems preferable.

The unequal distances of closest approach (UDCA) theory[12−14] represents the simplest theoretical extension of the classical Gouy−Chapman theory to account for individual distances of closest approach of all ions in solution. Though it leads to analytical solutions only in the case of two distinct planes of closest approach,[14] it has been successfully applied to the analysis of cationic adsorption,[15,16] and has provided a satisfactory explanation of some unusual double-layer effects on electrode kinetics.[17,18]

In this work, we have studied the rate of reduction of Zn^{2+} in the presence of $LiC1O_4$, $Mg(C1O_4)_2$, and $Al(ClO_4)_3$ solutions. These electrolytes were chosen since they provide a set of cations whose charge numbers and solvated radii embrace those of Zn^{2+}, they include a noncomplexing anion, and their distances of closest approach have been made available by a recent UDCA analysis of their surface excesses.[19] Moreover, these electrolytes are not specifically adsorbed in the potential range of interest, and they allow a straightforward comparison with previously published results that were obtained in the presence of $NaClO_4$. Values of the charge-transfer rate constants are derived from

* To whom correspondence should be addressed. E-mail: fondacab@cica.es.

10.1021/jp0113984 CCC: $20.00
Published on Web 09/15/2001

faradaic impedance measurements, since this electrochemical technique can provide accurate kinetic data over an extended potential range.[20,21]

The electrostatic boundary value problem, from which potential profiles are calculated, is solved within the framework of the orthogonal collocation technique. This computational technique offers the advantage of requiring fewer spatial points as compared to classical finite difference schemes to obtain the interfacial potential profile.

Theory

(a) Generalization of the UDCA Theory to the Case of an Electrolyte with *n* Planes of Closest Approach. An extension of the previously published UDCA theory[13,14] has been carried out to include *n* planes of closest approach. The electrode is modeled as a flat hard wall, and the primitive model is used to describe the solution side of the interface. Each *p* ion is defined by its number charge (z_p) and its distance of closest approach to the electrode surface (a_p).

The electrostatic potential distribution across the interface is obtained by solving the Poisson−Boltzmann (PB) equation

$$\frac{d^2\phi}{dx^2} = -\frac{e_o}{\epsilon}\sum_p z_p c_p^o H(x-a_p)\exp(-z_p\beta e_o\phi) \qquad (1)$$

where ϕ is the mean electrostatic potential at a distance x from the electrode surface and is measured with respect to the bulk (i.e., $\phi(\infty) = 0$), ϵ is the local dielectric permittivity, e_o is the electronic charge, c_p^o is the bulk concentration of ion p, $\beta = (kT)^{-1}$, and $H(x-a_p)$ is the Heaviside function

$$H(x-a_p) = \begin{cases} 0 & x < a_p \\ 1 & x \geq a_p \end{cases} \qquad (2)$$

which is introduced to restrict the access of the ions up to their distances of closest approach to the electrode.

To solve eq 1, the one-dimensional space is divided into a number of regions (NRE + 1), requiring that some of the inner borders between successive intervals coincide with the a_p values to avoid numerical discontinuities therein (Figure 1a). Each region is characterized by its dielectric permittivity (ϵ_I) and thickness (δ_I).

For the sake of computational convenience, the linearized form of the PB equation is adopted in the last region (extending from $x = h_{NRE}$ up to $x = \infty$):

$$\frac{d^2\phi}{dx^2} = \chi^2\phi \qquad (3)$$

where χ stands for the reciprocal of the Debye screening length

$$\chi = \left(\frac{e_o^2\beta}{\epsilon_{NRE+1}}\sum_p z_p^2 c_p^o\right)^{1/2} \qquad (4)$$

Integration of eq 3 gives

$$\phi(x \geq h_{NRE}) = \phi(h_{NRE})\exp[-\chi(x - h_{NRE})] \qquad (5)$$

This is a reasonable approximation as long as $\phi(h_{NRE}) \leq 2kT/ze_o$.[22] Thus, we have used this condition as a criterion for the choice of the h_{NRE} values.

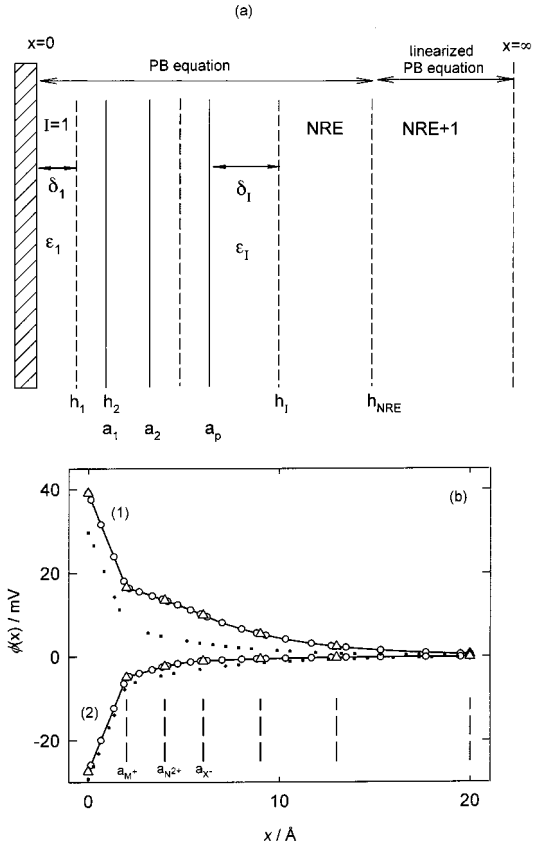

Figure 1. (a) Schematic representation of the interphase model used to solve the UDCA theory with *n* planes of closest approach within the orthogonal collocation framework. Vertical dashed and solid lines represent the border of the space intervals and distances of closest approach of each ion, respectively. (b) A typical potential profile obtained from the UDCA theory with three planes of closest approach for a mixture of two electrolytes, MX = 0.1 M and NX_2 = 0.1 M. The distances of closest approach of each ion to the electrode are a_{M^+} = 0.20 nm, $a_{N^{2+}}$ = 0.40 nm, and a_{X^-} = 0.60 nm. The dielectric permittivity for the first region is $\epsilon_1 = 10$, and for any other region $\epsilon_I = 78.5$. (1) $\sigma^M = 1\ \mu C\ cm^{-2}$. (2) $\sigma^M = -1\ \mu C\ cm^{-2}$. Vertical dashed lines indicate boundaries between the computational regions. Dotted lines represent the corresponding Gouy−Chapman profiles.

In the space extending from region $I = 1$ to region $I =$ NRE, the nonlinearized PB equation is solved by using the following outer boundary conditions:

$$x = 0: \quad \left(\frac{d\phi}{dx}\right)_{x=0^+} = -\frac{\sigma^M}{\epsilon_1} \qquad (6)$$

$$x = h_{NRE}: \quad \left(\frac{d\phi}{dx}\right)_{x=h_{NRE}} = -\chi\phi(h_{NRE}) \qquad (7)$$

where σ^M is the electrode charge density. The inner boundary conditions at the border between successive intervals are

$x = h_I$ ($I = 1$, NRE − 1):

$$\phi(h_I^-) = \phi(h_I^+) = \phi(h_I) \qquad (8)$$

$$\epsilon_I\left(\frac{d\phi}{dx}\right)_{x=h_I} = \epsilon_{I+1}\left(\frac{d\phi}{dx}\right)_{x=h_{I+1}} \qquad (9)$$

Equations 6 and 9 are derived from the Gauss theorem, and eq 7 results directly from eq 4. Integration of eq 1 subjected to the previous boundary conditions was accomplished by using

the orthogonal collocation technique, with six collocation points per region. Details of the derivative discretizations as well as of the solution of the resulting nonlinear equations may be found elsewhere.[23]

As an example, Figure 1b shows a typical potential profile for a mixture of two electrolytes with three planes of closest approach. The six boundaries between the computational regions selected are indicated by vertical bars. Circles and triangles represent the inner and outer collocation points in each region, respectively. As expected, potential profiles are not symmetrical with respect to the surface charge density due to the different distances of closest approach of the ions to the electrode. The presence of an ion-free layer close to the electrode, with a lower dielectric permittivity, results in a fast linear decay of the potential in the first region. As a visual reference, the corresponding Gouy−Chapman potential profile is also included (dotted lines).

(b) Frumkin Correction for the Bielectronic Zn^{2+} Reduction Mechanism. As stated before, the Zn^{2+} reduction mechanism is assumed to consist of a series of elementary steps, whose dependence on the interfacial potential distribution can be described as follows:

(1) Fast and reversible exchange of the Zn^{2+} ion between the bulk solution and its plane of closest approach to the electrode (rp1)

$$Zn^{2+}(\text{bulk}) \leftrightarrow Zn^{2+}(\text{rp1}) \tag{10}$$

The reactant concentration at rp1 is then related to its bulk value through

$$c^{\text{rp1}}_{Zn^{2+}}/c^{\text{bulk}}_{Zn^{2+}} = \exp(-2f\phi^{\text{rp1}}) \tag{11}$$

where $f = F/RT$ and ϕ^{rp1} is the average potential at rp1.

(2) Electron transfer and partial dehydration at rp1

$$Zn^{2+}(\text{rp1}) + e^{-}(\text{Hg}) \leftrightarrow Zn^{+}(\text{rp1}) \tag{12}$$

which satisfies under equilibrium conditions

$$c^{\text{rp1}}_{Zn^{2+}}/c^{\text{rp1}}_{Zn^{+}} = \exp[f(E - \phi^{\text{rp1}} - E^{\text{f}}_2)] = K^{\text{o}}_2 \exp[f(E - \phi^{\text{rp1}})] = K_2 \tag{13}$$

where E stands for the applied potential, E^{f}_2 stands for the formal potential of step 2, and K^{o}_2 represents the potential-independent contribution to the equilibrium constant K_2. The rate of electron transfer υ_2 can be expressed as

$$\upsilon_2 = k_{\text{f2}}c^{\text{rp1}}_{Zn^{2+}} - k_{\text{b2}}c^{\text{rp1}}_{Zn^{+}} = k_{\text{f2}}(c^{\text{rp1}}_{Zn^{2+}} - K_2c^{\text{rp1}}_{Zn^{+}}) \tag{14}$$

where k_{f2} and k_{b2} are the forward and backward electron-transfer rate constants, respectively, and

$$k_{\text{f2}} = k^{\text{o}}_{\text{f2}} \exp[-\alpha_2 f(E - \phi^{\text{rp1}})] = k_{\text{b2}}/K_2 \tag{15}$$

where α_2 is the cathodic transfer coefficient of the first electron transfer.

(3) Fast and reversible transfer of the short-lived Zn^{+} intermediate from the first to the second reaction plane (rp2)

$$Zn^{+}(\text{rp1}) \leftrightarrow Zn^{+}(\text{rp2}) \tag{16}$$

Under equilibrium conditions, Zn^{+} concentrations at rp1 and rp2 are related by

$$c^{\text{rp1}}_{Zn^{+}}/c^{\text{rp2}}_{Zn^{+}} = \exp[f(\phi^{\text{rp2}} - \phi^{\text{rp1}})] = K_3 \tag{17}$$

where ϕ^{rp2} is the average local potential at rp2.

(4) Second electron transfer and partial dehydration of Zn^{+} at rp2

$$Zn^{+}(\text{rp2}) + e^{-}(\text{Hg}) \leftrightarrow Zn(\text{rp2}) \tag{18}$$

which satisfies at equilibrium

$$c^{\text{rp2}}_{Zn^{+}}/c^{\text{rp2}}_{Zn} = \exp[f(E - \phi^{\text{rp2}} - E^{\text{f}}_4)] = K^{\text{o}}_4 \exp[f(E - \phi^{\text{rp2}})] = K_4 \tag{19}$$

and whose reaction rate is given by

$$\upsilon_4 = k_{\text{f4}}c^{\text{rp2}}_{Zn^{+}} - k_{\text{b4}}c^{\text{rp2}}_{Zn} = k_{\text{f4}}(c^{\text{rp2}}_{Zn^{+}} - K_4c^{\text{rp2}}_{Zn}) \tag{20}$$

with

$$k_{\text{f4}} = k^{\text{o}}_{\text{f4}} \exp[-\alpha_4 f(E - \phi^{\text{rp2}})] = k_{\text{b4}}/K_4 \tag{21}$$

where α_4 is the cathodic transfer coefficient of the second electron transfer.

(5) Fast and reversible Zn transfer from rp2 to the zinc amalgam

$$Zn(\text{rp2}) \leftrightarrow Zn(\text{Hg}) \tag{22}$$

which satisfies at equilibrium

$$c^{\text{rp2}}_{Zn}/c^{\text{Hg}}_{Zn} = K^{\text{o}}_5 \tag{23}$$

The experimentally available forward rate constant k_{f} for the overall reaction

$$Zn^{2+}(\text{bulk}) + 2e^{-}(\text{Hg}) \leftrightarrow Zn(\text{Hg}) \tag{24}$$

can be related to the forward rate constants of the two electron-transfer steps by adopting the steady-state hypothesis for the Zn^{+} intermediate, to give[21]

$$\frac{1}{k_{\text{f}}} = \frac{\exp(2f\phi^{\text{rp1}})}{k_{\text{f2}}} + \frac{\exp(f\phi^{\text{rp2}})}{k_{\text{f4}}} = \frac{\exp(2f\phi^{\text{rp1}})}{k_{\text{f2}}} + \frac{\exp(2f\phi^{\text{rp1}})}{K_2^{-1}K_3^{-1}k_{\text{f4}}} \tag{25}$$

Equation 25 can be rearranged to give corrected Frumkin plots as a function of the $E - \phi^{\text{rp1}}$ potential drop:[9]

$$\frac{\exp(-2f\phi^{\text{rp1}})}{k_{\text{f}}} = \frac{\exp[\alpha_2 f(E - \phi^{\text{rp1}})]}{k^{\text{o}}_{\text{f2}}} + \frac{K^{\text{o}}_2 \exp[(1 + \alpha_4)f(E - \phi^{\text{rp1}})]}{k^{\text{o}}_{\text{f4}} \exp[(1 - \alpha_4)f(\phi^{\text{rp1}} - \phi^{\text{rp2}})]} \tag{26}$$

This last equation differs from a similar expression reported in the literature[5] by the presence of the $\exp[(1 - \alpha_4)f(\phi^{\text{rp1}} - \phi^{\text{rp2}})]$ factor, which accounts for the change in the average local potential at the two planes where the electron transfers take place. Moreover, the potential dependence of the rate constants is expressed in terms of the rate constant at an arbitrary "zero potential", rather than in terms of the rate constant at the formal potential of the overall reaction. This choice is less convenient from a mathematical point of view, as it involves a far extrapolation to determine k^{o}_{f2} and k^{o}_{f4}, but it keeps a more clear connection with each separate electron-transfer step, since their formal potentials E^{f}_2 and E^{f}_4 are not accessible experimentally.

A satisfactory account of the Frumkin effect requires that the corrected kinetic parameters become independent of the nature and concentration of the supporting electrolyte. However, the comparison between the charge-transfer parameters obtained in the presence of two distinct electrolytes demands also a consideration of the corresponding changes in liquid junction potentials and activity coefficients. These changes will be considered later in more detail, but now we will show explicitly the influence of the activity coefficients on the rate and equilibrium parameters that appear in eq 26.

The charge-transfer rate constants for the two electron-transfer steps can be expressed as

$$k_{f2}^{o} = k_{f2}^{o'} \frac{\gamma_{Zn^{2+}}^{rp1}}{\gamma_{\neq,1}} \approx k_{f2}^{o'} \frac{\gamma_{Zn^{2+}}^{bulk}}{\gamma_{\neq,1}} = k_{f2}^{*} \gamma_{Zn^{2+}}^{bulk} \quad (27)$$

$$k_{f4}^{o} = k_{f4}^{o'} \frac{\gamma_{Zn^{+}}^{rp2}}{\gamma_{\neq,2}} \approx k_{f4}^{o'} \frac{\gamma_{Zn^{+}}^{rp1}}{\gamma_{\neq,2}} = k_{f4}^{*} \gamma_{Zn^{+}}^{rp1} \quad (28)$$

$$K_2^{o} = K_2^{*} \frac{\gamma_{Zn^{+}}^{rp1}}{\gamma_{Zn^{2+}}^{rp1}} \approx K_2^{*} \frac{\gamma_{Zn^{+}}^{rp1}}{\gamma_{Zn^{2+}}^{bulk}} \quad (29)$$

where $\gamma_{\neq,1}$ and $\gamma_{\neq,2}$ are the activity coefficients of the activated complexes, and it has been assumed that $\gamma_{Zn^{2+}}^{bulk} \approx \gamma_{Zn^{2+}}^{rp1}$ and $\gamma_{Zn^{+}}^{rp2} \approx \gamma_{Zn^{+}}^{rp1}$. Then, from eqs 28 and 29, it follows that

$$\frac{k_{f4}^{o}}{K_2^{o}} \approx \frac{k_{f4}^{*}}{K_2^{*}} \gamma_{Zn^{2+}}^{bulk} \quad (30)$$

By substituting eq 30 into eq 26, it follows that

$$\frac{\exp(-2f\phi^{rp1})}{k_f} = \frac{\exp[\alpha_2 f(E - \phi^{rp1})]}{k_{f2}^{*} \gamma_{Zn^{2+}}^{bulk}} + \frac{K_2^{*} \exp[(1 + \alpha_4) f(E - \phi^{rp1})]}{k_{f4}^{*} \gamma_{Zn^{2+}}^{bulk} \exp[(1 - \alpha_4) f(\phi^{rp1} - \phi^{rp2})]} \quad (31)$$

where k_{f2}^{*} and k_{f4}^{*} may retain some influence of the surrounding medium through the activity coefficients of the activated complexes. However, $\gamma_{\neq,1}$ and $\gamma_{\neq,2}$ will be assumed to be independent of the electrolyte nature and of the electrode potential, due to the lack of perchlorate specific adsorption at the rather negative potentials where the Zn^{2+} reduction takes place.[19]

Experimental Section

Measurements were performed in a three-electrode cell, with a platinum foil of high surface area as counter electrode, a saturated sodium chloride calomel electrode (SSCE), connected to the cell via a salt bridge containing the same solution as the cell, as reference electrode, and a modified EG&G PARC model 303A static mercury drop working electrode.

The lithium, magnesium, and aluminum perchlorate solutions were made up with Merck analytical grade reagents and water purified by a Millipore Milli-Q water system. The $Zn(ClO_4)_2$ solutions were prepared by dissolving ZnO in a small excess of perchloric acid to avoid hydrolysis of Zn^{2+}, making the final solution 10^{-3} M in H^{+}. The concentration of Zn^{2+} in the cell (6 or 20 mM) was chosen to optimize experimental accuracy over an extended potential range.

TABLE 1: Values of the Zn^{2+} Diffusion Coefficient, Zn^{2+}/Zn(Hg) Formal Potential, and Activity Coefficient for the Supporting Electrolytes Considered in the Text

Electrolyte	c/ (mol L^{-1})	$10^6 D_o$/ (cm^2 s^{-1})	$-E_f^o$/V vs SSCE	$-(\ln \gamma_{Zn^{2+}})$
$NaClO_4$[a]	0.20	7.1	0.997	1.057
	0.50	7.1	0.995	1.116
	1.00	6.6	0.991	1.009
$LiClO_4$	0.20	6.9	1.010	1.024
	0.50	6.7	1.004	1.038
	1.00	6.4	0.991	0.822
$Mg(ClO_4)_2$	0.10	7.3	1.006	1.116
	0.25	6.8	1.005	1.127
	0.50	6.2	0.991	0.847
$Al(ClO_4)_3$	0.07	6.8	1.003	1.189
	0.17	6.4	1.002	1.216
	0.35	5.7	0.989	0.927

[a] Data in the presence of $NaClO_4$ have been taken from ref 5, except for the activity coefficient values, which have been calculated in this work.

Oxygen was eliminated by bubbling nitrogen through the cell, which had been presaturated with the cell solution. Mercury was purified by treatment with diluted nitric acid and mercurous nitrate, and it was then distilled three times under vacuum. Cell impedances and dc polarograms were measured with the network analyzer described previously[24,25] at $t = 4$ s after the drop birth. The dc potential was corrected to account for the ohmic drop in the cell, when necessary. Experiments were carried out at 25 ± 0.1 °C using a Haake D8.G circulator thermostat.

Results and Discussion

Diffusion coefficients of Zn^{2+} in solution (D_O) have been obtained from the diffusion-limiting dc currents i_d, and are listed in Table 1. The value of the diffusion coefficient of zinc in the mercury amalgam, $D_R = 1.6\ 10^{-5}$ cm^2 s^{-1}, was taken from the literature.[26] Reversible half-wave potentials $E_{1/2}^{r}$ were determined by extrapoling the reversible part of the dc wave to $\ln[i/(i_d - i)] = 0$, in the $\ln[i/(i_d - i)]$ vs E plots. The formal potential values listed in Table 1 were then computed from $E_o^f = E_{1/2}^{r} + (RT/2F) \ln(D_O/D_R)^{1/2}$.

The frequency dependence of the cell impedance was fitted to a Randles equivalent circuit at each potential, but due to the sluggish charge-transfer kinetics that characterize Zn^{2+} reduction, the charge-transfer resistance (R_{ct}) was obtained with a higher accuracy than the Warburg coefficient. To determine k_f from the charge-transfer resistance, some functionality relating k_f and the electrode potential has to be assumed. Similar results were obtained in this work either when k_f was developed as a series of powers of electrode potential[5] or when the expected functionality for a two-electron-transfer mechanism was adopted.[21]

Figures 2 and 3 show the experimental charge-transfer resistance and rate constant values obtained by assuming a two-electron-transfer mechanism, as a function of the supporting electrolyte composition. The lines in Figure 2 illustrate how the variation of the charge-transfer rate constants with potential reproduces satisfactorily the measured charge-tranfer resistances. It is observed from Figure 3 that $\ln k_f$ decreases upon increasing the electrolyte concentration, and that it follows the sequence $\ln(k_f)_{Li^+} > \ln(k_f)_{Mg^{2+}} > \ln(k_f)_{Al^{3+}}$, at a given perchlorate concentration and electrode potential. To account quantitatively for these trends in terms of the UDCA theory, a rather detailed description of the interfacial structure has to be adopted first.

(a) UDCA Interfacial Structure. A recent theoretical analysis of the surface excesses of a series of chlorides and

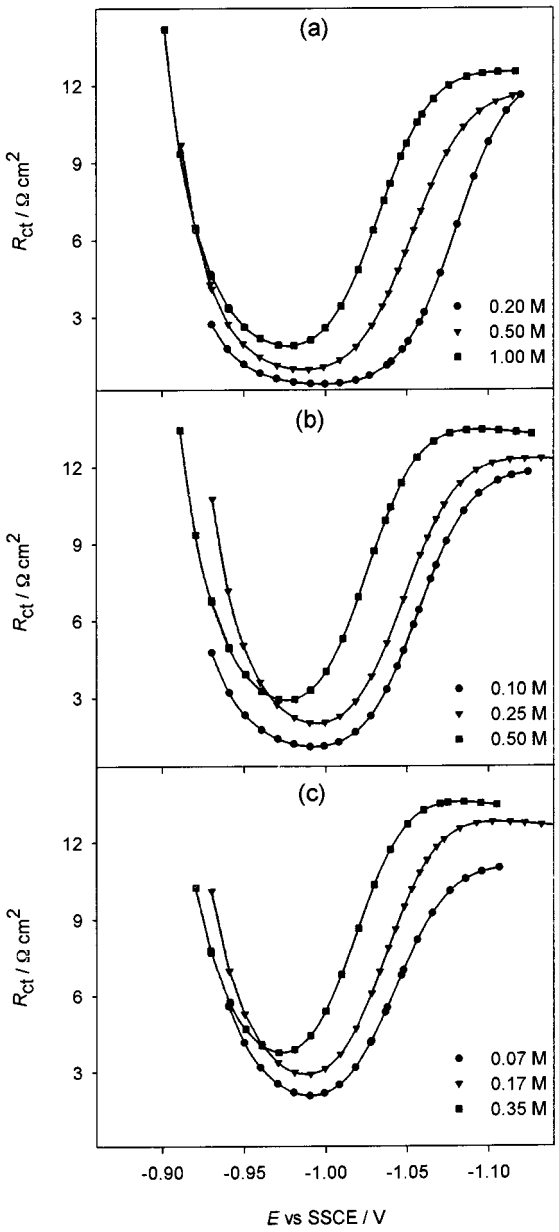

Figure 2. Charge-transfer resistance values obtained for the reduction of Zn^{2+} in the presence of (a) $LiClO_4$, (b) $Mg(ClO_4)_2$, and (c) $Al(ClO_4)_3$ solutions. Lines are theoretical fits for a two-electron-transfer mechanism.

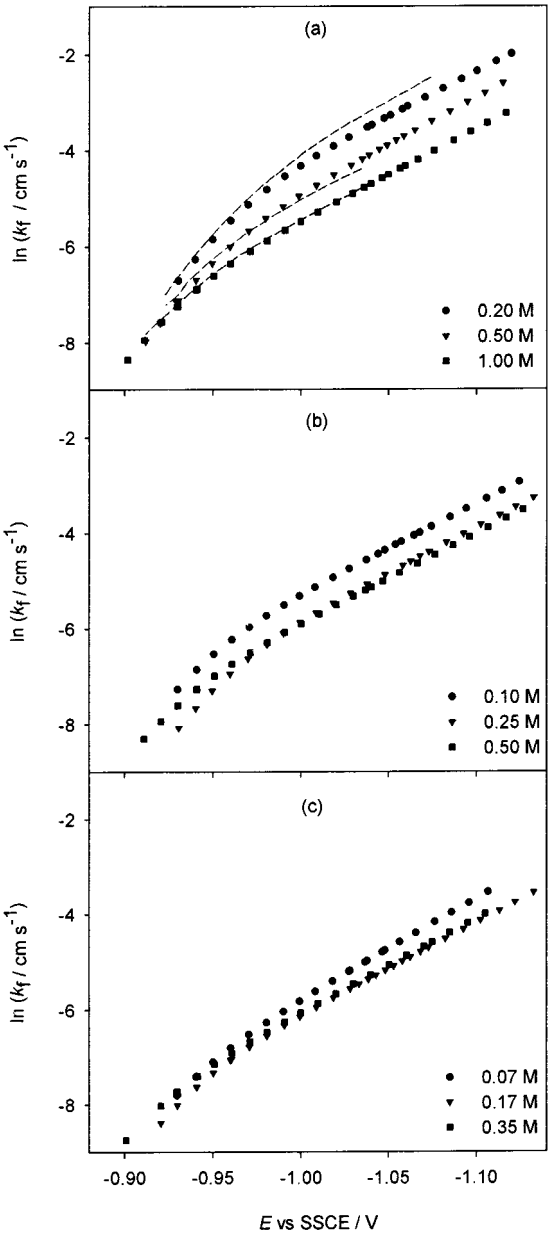

Figure 3. Charge-transfer rate constants for Zn^{2+} reduction derived from the R_{ct} values in Figure 2: (a) $LiClO_4$, (b) $Mg(ClO_4)_2$, and (c) $Al(ClO_4)_3$ solutions. Short dashed lines in (a) correspond to Zn^{2+} reduction in $NaClO_4$ solutions.[5]

perchlorates[19] has allowed the estimation of the individual distances of closest approach to the electrode surface of Li^+, Na^+, Mg^{2+}, Al^{3+}, and ClO_4^-, which are reproduced schematically in Figure 4. The distances of closest approach of the cations were found to be similar to their hydrated radii,[27] suggesting that cations share their solvation shell with the electrode, at least at the rather negative potentials where these results were obtained ($\sigma^M \approx -15\ \mu C\ cm^{-2}$). The larger distance of closest approach of perchlorate agrees with the presence of a water monolayer interposed between the anion and the electrode. Besides defining the charged components that populate each space region, the UDCA analysis also requires one to specify the interfacial dielectric profile. Satisfactory results have been obtained under a variety of conditions[14−19] by assuming a relative permittivity $\epsilon_3 = 78.5$ in the outer region where both cations and anions are present, and a lower value $\epsilon_2 = 33$ in the intermediate region where only cations (or anions) may enter.

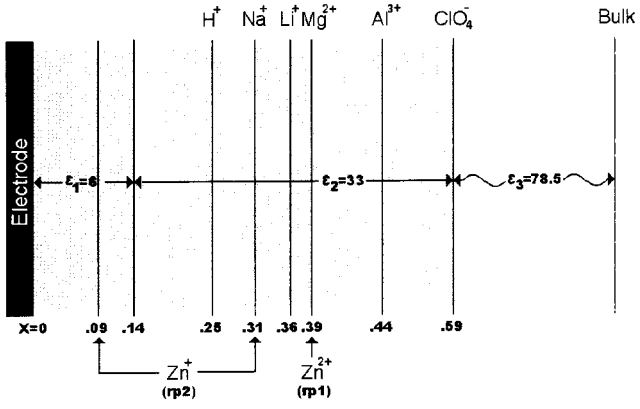

Figure 4. Schematic representation of the interphase showing the UDCA distances of closest approach to the electrode for Li^+, Na^+, Mg^{2+}, Al^{3+}, and ClO_4^-, and the dielectric permittivity profile. The location of the two electron-transfer planes (rp1 and rp2) are also indicated.

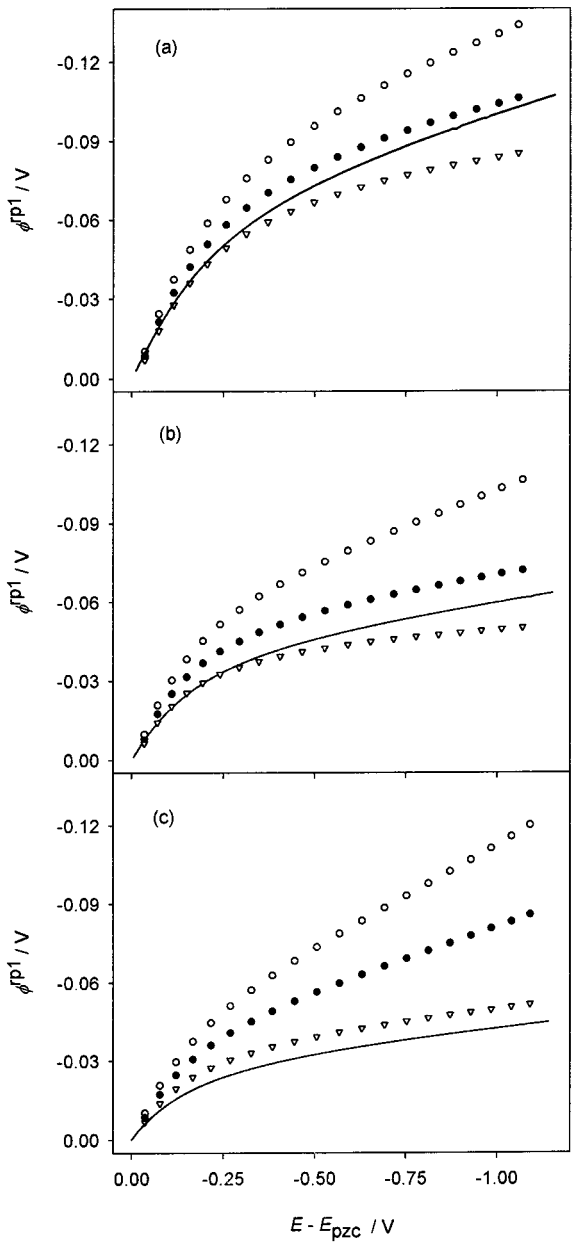

Figure 5. Local average potential values at the plane of closest approach of Zn^{2+} (ϕ^{rp1}), in the presence of the following supporting electrolytes: (a) 0.2 M $LiClO_4$, (b) 0.1 M $Mg(ClO_4)_2$, and (c) 0.07 M $Al(ClO_4)_3$. Lines were computed from the Gouy−Chapman (ϕ^{GC}) theory. Solid symbols were computed from the UDCA theory with a distance of closest approach of 0.39 nm. Open symbols were estimated from the UDCA theory assuming that $a_{Zn^{2+}} = 0.39 + 0.05$ nm (▽) or that $a_{Zn^{2+}} = 0.39 - 0.05$ nm (○).

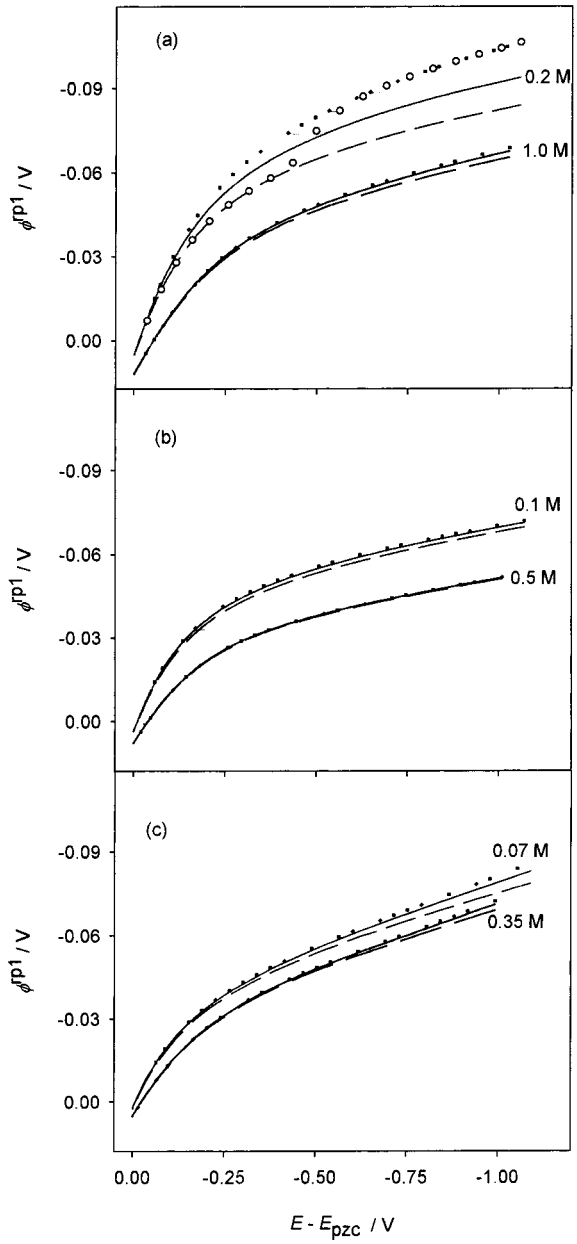

Figure 6. Influence of $Zn(ClO_4)_2$ concentration on the potential at the plane of closest approach of Zn^{2+} (ϕ^{rp1}), in the presence of the following supporting electrolytes: (a) $LiClO_4$, (b) $Mg(ClO_4)_2$, and (c) $Al(ClO_4)_3$. Dotted lines were computed from the UDCA theory in the absence of $Zn(ClO_4)_2$. Solid and dashed lines show the variation of ϕ^{rp1} upon addition of 6 and 20 mM $Zn(ClO_4)_2$, respectively. Supporting electrolye concentrations are also indicated. Circles in (a) illustrate the effect of electrolytic depletion of Zn^{2+} in a 20 mM $Zn(ClO_4)_2$ and 0.2 M $LiClO_4$ solution. Distances of closest approach and permittivity values are as in Figure 4.

The latter value results from averaging the Levine and Fawcett dielectric profile[28] between the low-field limit $\epsilon_3 = 78.5$, which applies to the classical diffuse layer, and the high-field limit $\epsilon_1 = 6$,[29] which applies between the electrode surface and the plane of closest approach of the solvent molecules, i.e., within a solvent slab of 0.14 nm thickness.

To study the kinetics of Zn^{2+} reduction, experiments were performed in the presence of an excess of supporting electrolyte ($LiClO_4$, $Mg(ClO_4)_2$, or $Al(ClO_4)_3$), but also with two additional electrolytes, namely, $HClO_4$ and $Zn(ClO_4)_2$. Zinc perchlorate was the source of the electroactive Zn^{2+} cations, and its concentration was either 6 or 20 mM, whereas perchloric acid was added to prevent Zn^{2+} hydrolysis, and its concentration was always 1 mM. These two electrolytes increase the overall perchlorate concentration, but also introduce two additional cations with their own distances of closest approach to the electrode. First, we will consider how the electrolyte composition affects the two electrostatic factors ϕ^{rp1} and ($\phi^{rp1} - \phi^{rp2}$) in eq 26, and then we will analyze the observed Frumkin effect on the rate of Zn^{2+} reduction.

Due to the lack of appropriate electrocapillary data, some assumptions have to be adopted in relation to the distances of closest approach of Zn^{2+}, H^+, and Zn^+. Thus, we have assumed that Zn^{2+} has the same distance of closest approach as Mg^{2+}

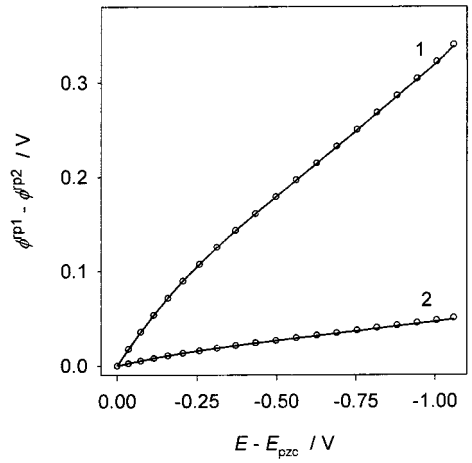

Figure 7. Potential drop between the two planes of electron transfer $\phi^{rp1} - \phi^{rp2}$ as a function of the electrode potential, in the presence of the 0.2 M $LiClO_4$. Curves 1 and 2 correspond to $a_{Zn^+} = 0.09$ nm and $a_{Zn^+} = 0.31$ nm, respectively.

(i.e., $a_{Zn^{2+}} = a_{Mg^{2+}} = 0.39$ nm), since their charge numbers are identical and their hydrated radii are very similar.[27] The solid symbols in Figure 5 show the UDCA potential at rp1 in 0.2 M $LiClO_4$, 0.1 M $Mg(ClO_4)_2$, and 0.07 M $Al(ClO_4)_3$ solutions. In all cases, the UDCA potential is more negative than the diffuse layer potential drop estimated from the Gouy−Chapman theory (solid lines). The difference between these two sets of values increases with the cationic distance of closest approach, reflecting a progressive loss of ionic screening at the reaction plane. The sensitivity of rp1 toward a change of ±0.05 nm in the Zn^{2+} distance of closest approach is also illustrated (open symbols in Figure 5).

The additional presence of 1 mM $HClO_4$ in solution has a negligible influence on ϕ^{rp1}, when the distance of closest approach of H^+ is assumed to be ≥0.25 nm, the estimated value for H^+ from the linear correlation between cationic hydrated radii and distances of closest approach.[19]

We have also explored the influence of $Zn(ClO_4)_2$ concentration on ϕ^{rp1} (Figure 6). The absolute value of ϕ^{rp1} is observed to decrease upon increasing the reactant concentration, although this effect appears to be relevant only in the case of the most diluted $LiClO_4$ solution, Figure 6a. Even in this case, the presence of the electrolytic process results in a progressive decrease of the Zn^{2+} concentration in the vicinity of the electrode surface as the potential is made more negative. The changes in the ϕ^{rp1} values are restricted to less than 5 mV when the $Zn(ClO_4)_2$ concentration is varied from 6 to 20 mM, in agreement with the observed lack of dependence of k_f with respect to Zn^{2+} concentration.

To locate the plane of the second electron transfer, we have envisaged two alternatives. Either Zn^+ shares its solvation shell with the electrode, as alkali-metal cations seem to do, or it loses part of its solvation shell to become contact-adsorbed on the electrode surface. In the first case, the distance of closest approach of Zn^+ has been assumed to be equal to that of Na^+, since they have similar values of the bare ion radius and charge, i.e., $a_{Zn^+} = a_{Na^+} = 0.31$ nm.[19] In the second case, the distance of closest approach of Zn^+ has been identified with its nonsolvated radius, i.e., $a_{Zn^+} = 0.09$ nm.[8]

Figure 7 illustrates how the $\phi^{rp1} - \phi^{rp2}$ potential drop increases with electrode potential. It may be observed that, at a given electrode potential, $\phi^{rp1} - \phi^{rp2}$ becomes more positive as the plane for the second electron transfer approaches the electrode surface (curve 1). Therefore, a higher stabilization of the monovalent intermediate, associated with larger $\phi^{rp1} - \phi^{rp2}$ values, is predicted when Zn^+ is allowed to come into contact with the electrode surface. This is the type of result to be expected from a purely electrostatic model, but it should be remembered that a precise determination of the Zn^+ free energy minimum in the reaction coordinate would require a full description of the ion−solvent and ion−electrode interaction energies, and is beyond the scope of this paper. On the other hand, the $Zn(ClO_4)_2$ concentration was found to have very little influence on the $\phi^{rp1} - \phi^{rp2}$ potential drop (not shown).

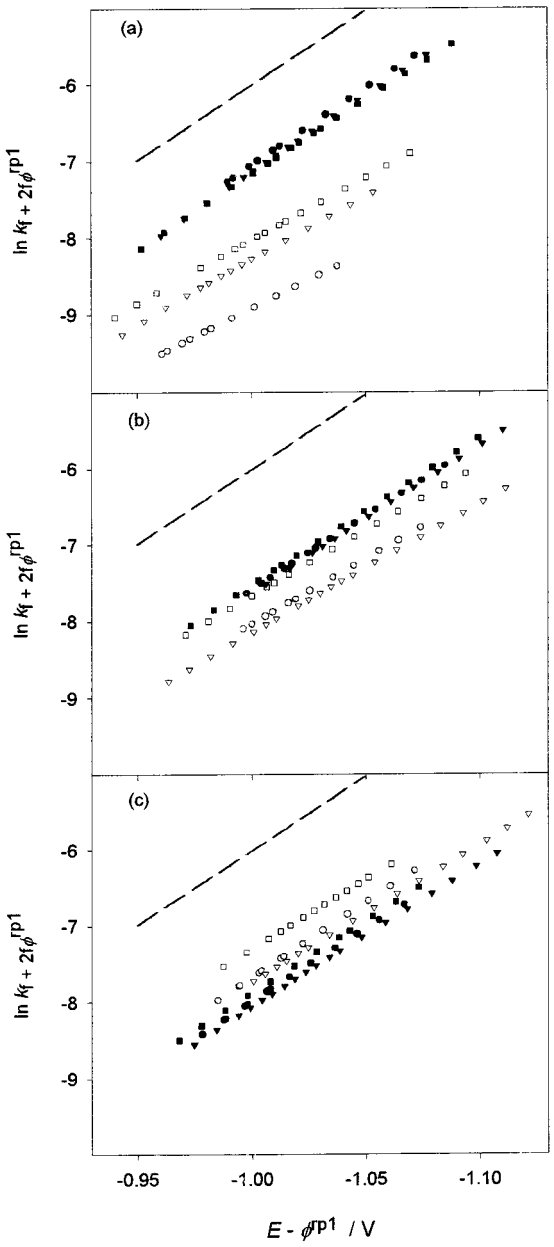

Figure 8. Corrected Frumkin plots for the first electron transfer of Zn^{2+} reduction, in the presence of (a) $LiClO_4$, (b) $Mg(ClO_4)_2$, and (c) $Al(ClO_4)_3$ electrolyte solutions: (○, ●) 0.2 M, (▽, ▼) 0.5 M, and (□, ■) 1.0 M perchlorate concentration. ϕ^{rp1} values were computed from the Gouy−Chapman theory (open symbols) and UDCA theory (solid symbols) with $a_{Zn^{2+}} = 0.39$ nm and $a_{H^+} = 0.25$ nm. All other distances of closest approach and permittivity values are indicated in Figure 4. Dashed lines are guidelines corresponding to $\alpha_2 = 0.5$.

(b) UDCA Correction of the Frumkin Effect. At sufficiently negative potentials, where the first electron transfer

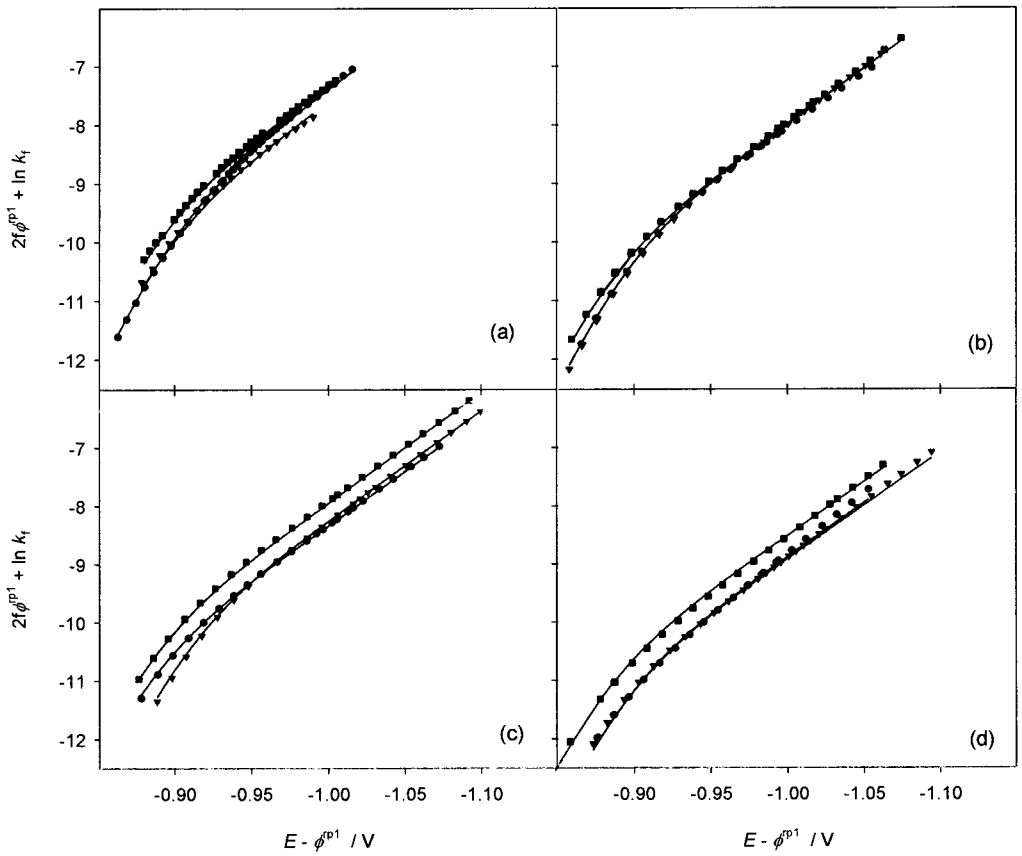

Figure 9. Corrected Frumkin plots for the Zn^{2+} reduction, in the presence of the supporting electrolytes (a) $NaClO_4$, (b) $LiClO_4$, (c) $Mg(ClO_4)_2$, and (d) $Al(ClO_4)_3$: (●) 0.20 M, (▼) 0.50 M, and (■) 1.0 M perchlorate concentration. ϕ^{rp1} and ϕ^{rp2} values were computed from the UDCA theory with $a_{Zn^{2+}} = 0.39$ nm, $a_{Zn^{+}} = 0.09$ nm, and $a_{H^{+}} = 0.25$ nm. All other distances of closest approach and permittivity values are indicated in Figure 4. Solid lines were computed from eq 26 and the parameter values in Table 2. Uncorrected rate constants in (a) were taken from ref 5.

TABLE 2: UDCA-Corrected Kinetic Parameters

Electrolyte	c/(mol L^{-1})	α_2[a]	$-\ln[k^o_{f2}/(\text{cm s}^{-1})]$[a]	α_4[b]	$\ln[(K^o_2)^{-1}[k^o_{f4}/(\text{cm s}^{-1})]]$	α_4[c]	$\ln[(K^o_2)^{-1}[k^o_{f4}/(\text{cm s}^{-1})]]$
$NaClO_4$	0.20	0.50	26.7	0.50	65.2	0.56	64.4
	0.50	0.49	26.8	0.50	65.0	0.57	64.4
	1.00	0.50	26.7	0.51	64.8	0.59	64.4
$LiClO_4$	0.20	0.48	26.8	0.49	65.2	0.56	64.5
	0.50	0.48	26.8	0.49	65.2	0.56	64.5
	1.00	0.48	26.8	0.50	65.0	0.56	64.1
$Mg(ClO_4)_2$	0.10	0.47	26.8	0.49	65.2	0.56	64.5
	0.25	0.48	26.9	0.47	65.4	0.54	64.5
	0.50	0.48	26.8	0.51	65.3	0.56	64.3
$Al(ClO_4)_3$	0.07	0.47	27.3	0.49	66.0	0.56	65.2
	0.17	0.47	27.1	0.49	66.0	0.56	65.2
	0.35	0.47	26.9	0.51	66.6	0.58	65.0

[a] Values obtained from the slopes and intercepts shown in Figure 8. [b] Assuming $a_{Zn^{+}} = 0.09$ nm. [c] Assuming $a_{Zn^{+}} = 0.31$ nm.

becomes rate determining, a simplified version of the rate eq 26 can be adopted

$$\frac{\exp(-2f\phi^{rp1})}{(k_f)_{E\to-\infty}} \approx \frac{\exp[\alpha_2 f(E-\phi^{rp1})]}{k^o_{f2}} \qquad (32)$$

which includes two kinetic parameters only (α_2 and k^o_{f2}), and allows for a straightforward analysis of the Frumkin correction by plotting $2f\phi^{rp1} + \ln k_f$ vs $E - \phi^{rp1}$ (corrected Frumkin plot). Two sets of corrected Frumkin plots, where ϕ^{rp1} has been computed either from classical GC theory (open symbols) or from UDCA theory (solid symbols), are compared in Figure 8. As indicated above, an adequate account of the Frumkin effect should provide α_2 and k^o_{f2} values independent of the concentration and nature of the supporting electrolyte. In all cases, straight lines with slope values close to $\alpha_2 \approx 0.5$ were found. However, Gouy−Chapman corrected rate constants, which do not account for different distances of closest approach, display a systematic increase with electrolyte concentration and charge number of the electrolyte cation.

On the other hand, the UDCA theory gives more consistent results, mainly in the presence of 1:1 supporting electrolytes. UDCA-corrected rate constants are the same for the $LiClO_4$ solutions studied in this work (Figure 8a) and for those obtained in the presence of $NaClO_4$[5] (see Figure 9a and Table 2). Reasonable agreement is also found with the UDCA-corrected rate constants determined from $Mg(ClO_4)_2$ solutions (Figure 8b), but systematically lower rate constants are obtained in the

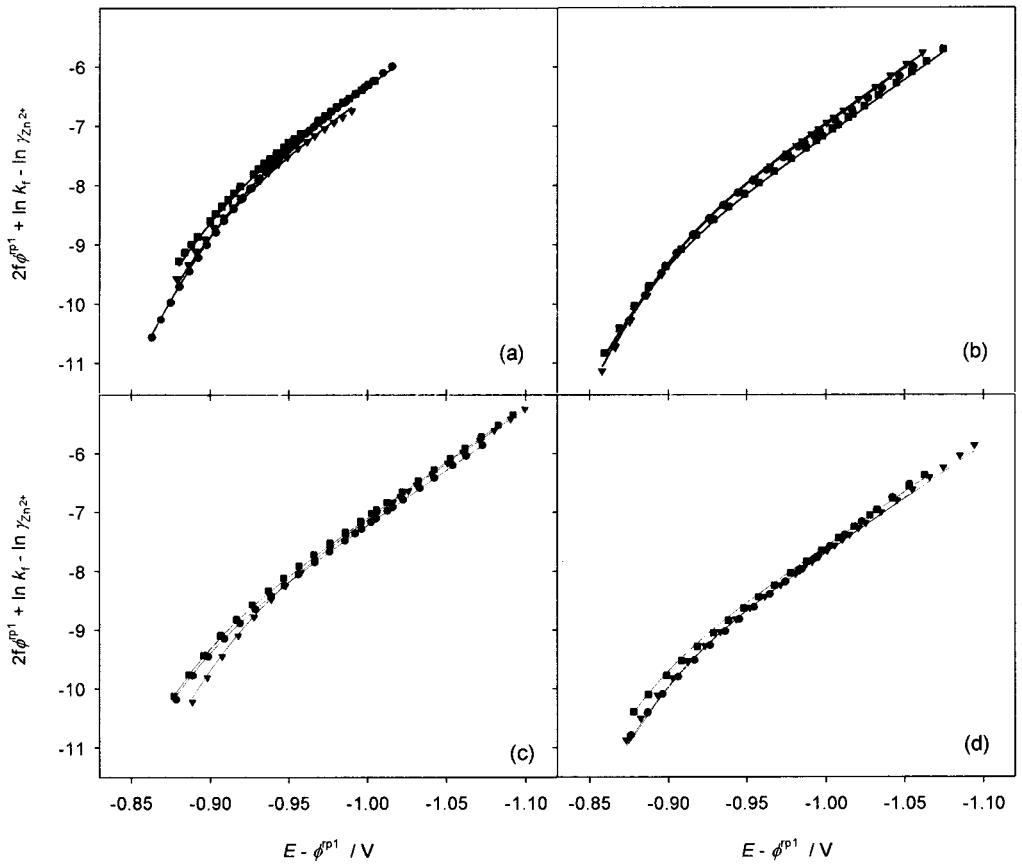

Figure 10. Corrected Frumkin plots for the Zn^{2+} reduction including the variation of the Zn^{2+} activity coefficient $\gamma^{bulk}_{Zn^{2+}}$ with solution composition, in the presence of the supporting electrolytes: (a) $NaClO_4$, (b) $LiClO_4$, (c) $Mg(ClO_4)_2$, and (d) $Al(ClO_4)_3$: (●) 0.2 M, (▼) 0.5 M, and (■) 1.0 M perchlorate concentration. ϕ^{rp1} and ϕ^{rp2} values were computed from the UDCA theory with $a_{Zn^{2+}} = 0.39$ nm, $a_{Zn^+} = 0.09$ nm, and $a_{H^+} = 0.25$ nm. All other distances of closest approach and permittivity values are indicated in Figure 4. Solid lines were computed from eq 31 and the parameter values in Table 3. Uncorrected rate constants in (a) were taken from Andreu et al.[5] Activity coefficients of Zn^{2+} were estimated from the MSA theory, as explained in the text.

TABLE 3: UDCA-Corrected Kinetic Parameters Taking into Account the Variation of the Zn^{2+} Activity Coefficient

Electrolyte	c/ (mol L^{-1})	α_2	$-\ln[k^*_{f2}/$ (cm s^{-1})]	α_4	$\ln[(K^*_2)^{-1}[k^*_{f4}/$ (cm s^{-1})]]
$NaClO_4$	0.20	0.50	25.6	0.50	64.1
	0.50	0.49	25.7	0.50	63.9
	1.00	0.50	25.7	0.51	63.8
$LiClO_4$	0.20	0.48	25.8	0.49	64.2
	0.50	0.48	25.8	0.49	64.2
	1.00	0.48	26.0	0.50	64.2
$Mg(ClO_4)_2$	0.10	0.47	25.7	0.49	64.1
	0.25	0.48	25.8	0.47	64.3
	0.50	0.48	26.0	0.51	64.5
$Al(ClO_4)_3$	0.07	0.47	26.1	0.49	64.8
	0.17	0.47	25.9	0.49	64.8
	0.35	0.47	26.0	0.51	64.7

presence of $Al(ClO_4)_3$ solutions (Figure 8c). The α_2 and k^o_{f2} values derived from the intercepts and slopes of these Frumkin-corrected plots are collected in Table 2. It can be seen that α_2 takes an average value of 0.48($\pm$0.02), close to the 1/2 expected for a simple outer-sphere electron transfer. A common value of $\ln[k^o_{f2}/(\text{cm s}^{-1})] = -26.8(\pm 0.1)$ reproduces the kinetic behavior in the presence of $LiClO_4$, $NaClO_4$, and $Mg(ClO_4)_2$ solutions, whereas a somewhat lower value of $\ln[k^o_{f2}/(\text{cm s}^{-1})] = -27.1(\pm 0.2)$ corresponds to the $Al(ClO_4)_3$ solutions.

Before extension of the Frumkin correction toward more positive potentials is attempted, the plane of the second electron transfer has to be specified. This plane is identified as the plane of closest approach of Zn^+, and as stated previously, we will assume that either the distance of closest approach of Zn^+ is determined by its solvation shell ($a_{Zn^+} = 0.31$ nm) or it loses part of its solvation shell and becomes contact-adsorbed on the electrode surface ($a_{Zn^+} = 0.09$ nm). Either of these two alternatives can reproduce satisfactorily the potential dependence of the corrected rate constants (see Table 2 and Figure 9), although they correspond to somewhat different values of the kinetic parameters α_4 and $(K^o_2)^{-1}k^o_{f4}$. Thus, in the presence of $LiClO_4$, $NaClO_4$, and $Mg(ClO_4)_2$ solutions, the average values of α_4 and $\ln[(K^o_2)^{-1}[k^o_{f4}/(\text{cm s}^{-1})]]$ change from 0.49($\pm$0.02) to 0.56($\pm$0.02) and from $-65.1(\pm 0.3)$ to $-64.4(\pm 0.3)$, respectively, as a_{Zn^+} is varied from 0.09 to 0.31 nm. As was observed for the first electron transfer, the kinetic parameter $(K^o_2)^{-1}k^o_{f4}$ takes slightly higher values in the most concentrated solutions for any electrolyte, and somewhat lower values in $Al(ClO_4)_3$ solutions. It should be noted that the kinetic term corresponding to the second electron transfer in eq 26 should not coincide for each solution when plotted in $2f\phi^{rp1} + \ln k_f$ vs $E - \phi^{rp1}$ coordinates, due to the presence of the $\exp[(1 - \alpha_4)f(\phi^{rp1} - \phi^{rp2})]$ factor.

When corrected rate constants are compared at a given potential, changes in liquid junction potentials and activity coefficients should also be considered. The heteroionic liquid junctions used in this work are not easily amenable to a theoretical analysis, but this is not the case for the Zn^{2+} reduction in the presence of $NaClO_4$ solutions,[5] which included homoionic liquid junctions between the working solution and a 3.0 M

TABLE 4: Optimized Values of $(r_i^{bulk})_{c\to 0}$ and the β and α Parameters in Eqs 33 and 34, Accounting for the Change in Ionic Radius and Solution Permittivity with Electrolyte Concentration

Ion	$(r_i^{bulk})_{c\to 0}$ /nm	β/(nm L mol^{-1})	α/(L mol^{-1})
Na^+	0.195	−0.00140	0.1023
Li^+	0.305	−0.00729	0.2123
Zn^{2+}	0.385	−0.01589	0.0963
Mg^{2+}	0.405	−0.01901	0.1719
Al^{3+}	0.495	−0.03534	0.2621
ClO_4^-	0.198	0	0

$NaClO_4$ solution. Dorta-Rodríguez et al.[30] carried out a detailed study of this liquid junction, and estimated a liquid junction potential variation of 7 mV between the 0.1 and 1.0 M $NaClO_4$ solutions. This estimate implies a modest additional dispersion of 0.3 unit in our previous ln k_{f2}^o values (see Table 2 and Figure 9a). Moreover, the close agreement between corrected rate parameters obtained in the presence of different electrolyte stoichiometries and types of liquid junction suggests that changes in the liquid junction potentials do not contribute significantly to the observed kinetic behavior, except perhaps in the case of $Al(ClO_4)_3$ solutions.

We have also explored the influence that the supporting electrolyte exerts on the reduction rate through the changes it induces in the Zn^{2+} activity coefficient $\gamma_{Zn^{2+}}^{bulk}$. Activity coefficients were computed from the MSA theory applied to the extended primitive model,[31] in which the ion radius r_i^{bulk} and solution permittivity ϵ^{bulk} were allowed to vary with electrolyte concentration according to

$$r_i^{bulk} = (r_i^{bulk})_{c\to 0} + \beta c \tag{33}$$

$$\epsilon^{bulk} = (\epsilon)_{c\to 0}/(1 + \alpha c) \tag{34}$$

where c is the molar electrolyte concentration, $(r_i^{bulk})_{c\to 0}$ is the ionic radius at infinite dilution, $(\epsilon)_{c\to 0}$ is the solvent permittivity, and α and β are fitting parameters accounting for the concentration dependence of r_i^{bulk} and ϵ^{bulk}. First, tabulated mean activity coefficients[32,33] of $NaClO_4$, $LiClO_4$, $Mg(ClO_4)_2$, $Zn(ClO_4)_2$, and $Al(ClO_4)_3$ were fitted to the MSA expressions. Then, trace activity coefficients of Zn^{2+} in the presence of an excess of supporting electrolyte were computed as described in the literature.[31,34] The optimized $(r_i^{bulk})_{c\to 0}$, α, and β values are gathered in Table 4, and the resulting Zn^{2+} activity coefficients are included in Table 1.

According to eq 31, corrected Frumkin plots that account for changes in the Zn^{2+} activity coefficient can be obtained by simply subtracting ln $\gamma_{Zn^{2+}}^{bulk}$ from the ordinate. It may be observed from Figure 10 and Table 3 how the explicit consideration of the changes in $\gamma_{Zn^{2+}}^{bulk}$ decreases significantly the scatter of the corrected rate constants for all the electrolytes considered in this work, and it also reduces the differences between the kinetic parameter values obtained in $Al(ClO_4)_3$ solutions and in other solutions. Therefore, a set of values can be assigned to the kinetic parameters $\alpha_2 = 0.48(\pm 0.02)$, $\ln[k_{f2}^*/(\text{cm s}^{-1})] = -25.8(\pm 0.2)$, $\alpha_4(a_{Zn^{2+}} = 0.09\ \text{nm}) = 0.49(\pm 0.02)$, and $\ln[(K_2^*)^{-1}[k_{f4}^*/(\text{cm s}^{-1})]](a_{Zn^{2+}} = 0.09\ \text{nm}) = -64.3(\pm 0.5)$ (see Table 3), which can be considered as independent of the concentration and nature of the supporting electrolyte.

Conclusions

An application of the orthogonal collocation technique to the numerical solution of the UDCA theory for any number of electrolytes and distances of closest approach has been developed. The observed Frumkin effect on the reduction rate of Zn^{2+}, in the presence of $NaClO_4$, $LiClO_4$, $Mg(ClO_4)_2$, and $Al(ClO_4)_3$ electrolyte solutions, has been analyzed in terms of a two consecutive electron transfer mechanism. Even though the plane where the second electron transfer takes place could be located only tentatively, a reasonable account of the Frumkin effect is obtained from the UDCA theory with ionic distances of closest approach derived independently from electrocapillary measurements. The consistency of the corrected rate constants can be further improved by considering the changes in the activity coefficient of Zn^{2+}, as estimated from the MSA theory within the framework of the extended primitive model of the electrolyte solutions.

Acknowledgment. We are indebted to Professor W. R. Fawcett for his valuable suggestions. This work has been supported by the Dirección General de Investigación Científica y Tecnológica (DGICYT) under Grant PB098-1123.

References and Notes

(1) Fawcett, W. R.; Lasia, A. *J. Electroanal. Chem.* **1990**, *279*, 243.
(2) Fawcett, W. R. *J. Electroanal. Chem.* **1991**, *302*, 13.
(3) Hurlen, T.; Eriksrud, E. *J. Electroanal. Chem.* **1973**, *45*, 405.
(4) Van der Pol, F.; Sluyters-Rehbach, M.; Sluyters, J. H. *J. Electroanal. Chem.* **1975**, *58*, 177.
(5) Andreu, R.; Sluyters-Rehbach, M.; Remijnse, A. G.; Sluyters, J. H. *J. Electroanal. Chem.* **1982**, *134*, 101.
(6) Pérez, M.; Baars, A.; Zevenhuizen, S. J. M.; Sluyters-Rehbach, M.; Sluyters, J. H. *J. Electroanal. Chem.* **1995**, *397*, 87.
(7) Schmickler, W. *Electrochim. Acta* **1996**, *41*, 2329.
(8) Pecina, O.; Schmickler, W. *Chem. Phys.* **2000**, *252*, 349.
(9) Fawcett, W. R. In *Electrocatalysis (Frontiers of Electrochemistry)*; Lipkowski, J., Ross, P. N., Eds.; Wiley-VCH: New York, 1998; Chapter 8.
(10) Fawcett, W. R. *Can. J. Chem.* **1981**, *59*, 1844.
(11) De Kreuk, C. W.; Sluyters-Rehbach, M.; Sluyters, J. H. *J. Electroanal. Chem.* **1970**, *28*, 391.
(12) Joshi, K. M.; Parsons, R. *Electrochim. Acta* **1961**, *4*, 129.
(13) Valleau, J. P.; Torrie, G. M. *J. Chem. Phys.* **1982**, *76*, 4623.
(14) Andreu, R.; Molero, M.; Calvente, J. J.; Carbajo, J. *J. Electroanal. Chem.* **1993**, *58*, 49.
(15) Molero, M.; Andreu, R. *J. Electroanal. Chem.* **1989**, *260*, 405.
(16) Molero, M.; Andreu, R. *J. Electroanal. Chem.* **1989**, *260*, 417.
(17) Damaskin, B. B.; Safonov, V. A.; Fedorovich, N. V. *J. Electroanal. Chem.* **1993**, *349*, 1.
(18) Ferapontova, E. E. *J. Electroanal. Chem.* **1999**, *476*, 37.
(19) López-Pérez, G.; González-Arjona, D.; Molero, M.; Andreu, R. *Langmuir* **1999**, *15*, 4892.
(20) Bongenaar, C. P. M.; Sluyters-Rehbach, M.; Sluyters, J. H. *J. Electroanal. Chem.* **1980**, *109*, 23.
(21) Bongenaar, C. P. M.; Remijnse, A. G.; Sluyters-Rehbach, M.; Sluyters, J. H. *J. Electroanal. Chem.* **1980**, *111*, 139.
(22) Bard, A. J.; Faulkner, L. R. *Electrochemical Methods Fundamental and Applications*; J. Wiley & Sons: New York, 1980; p 505.
(23) Calvente, J. J.; Andreu, R.; Gil, M. A.; González, L.; Alcudia, A.; Domínguez, M. *J. Electroanal. Chem.* **2000**, *482*, 18.
(24) Andreu, R.; González-Arjona, D.; Domínguez, M.; Molero, M.; Roldán, E. *Electroanalysis* **1991**, *3*, 377.
(25) González-Arjona, D.; López-Pérez, G.; Mozo, J. D.; Roldán, E. *Electroanalysis* **2000**, *12*, 1143.
(26) Stromberg, A. G. *Dokl. Akad. Nauk USSR* **1952**, *85*, 831.
(27) Nightingale, E. R. *J. Phys. Chem.* **1959**, *63*, 1382.
(28) Levine, S.; Fawcett, W. R. *J. Electroanal. Chem.* **1979**, *99*, 265.
(29) Yeh, I.-C.; Berkowitz, M. L. *J. Chem. Phys.* **1999**, *110*, 7935.
(30) Dorta-Rodríguez, R.; Barrera-Niebla, M.; González, S.; Hernández-Luis, F. *J. Electroanal. Chem.* **1997**, *436*, 173.
(31) Simonin, J. P. *J. Phys. Chem. B* **1997**, *101*, 4313.
(32) Robinson, R. A.; Stokes, R. H. *Electrolyte Solutions*, 2nd ed.; Butterworth: London, 1970.
(33) Molero, M.; González-Arjona, D.; Calvente, J. J.; López-Pérez, G. *J. Electroanal. Chem.* **1999**, *460*, 100.
(34) López-Pérez, G.; González-Arjona, D.; Molero, M. *J. Electroanal. Chem.* **2000**, *480*, 9.